Performance Analysis of an Induction Machine-Based Flywheel Energy Storage System Associated to a Variable-Speed Wind Generator

Gabriel Cimuca[1,2], Mircea M. Rădulescu[1],
Christophe Saudemont[2], Benoît Robyns[2]

(1) Small Electric Motors and Electric Traction (SEMET) Group, Technical University of Cluj-Napoca
P.O. Box 345, RO-400110 Cluj-Napoca 1, Romania,
E-mail : mircea.radulescu@mae.utcluj.ro
(2) Laboratoire d'Electrotechnique et d'Electronique de Puissance de Lille (L2EP)
Ecole des Hautes Etudes d'Ingénieur (HEI) 13, rue de Toul, F-59046 Lille Cedex, France
E-mail : benoit.robyns@hei.fr

***Abstract* – The flywheel energy storage systems (FESSs) are suitable for improving the quality of the electric power delivered by the wind generators and to help these generators to contribute to the ancillary services. This paper investigates the energetic performances of a low-speed FESS with a classical squirrel-cage Induction Machine (IM) in the aim of its association to a wind generator.**

***Index Terms* – Low-speed flywheel, energy storage, wind generator, losses, efficiency.**

I. INTRODUCTION

In the last years, Flywheel Energy Storage Systems (FESSs) have been rediscovered by the industrials due to their advantages in comparison with other energy storage systems [1]. FESSs have thus found a specific application for the electric power quality, as far as the voltage and frequency maintenance between imposed limits is concerned. By virtue of their high dynamics, long lifetime and good efficiency, FESSs are well suited for short-term storage systems, which are generally sufficient to improve the electric power quality [1]. In the case of variable-speed wind generators (VSWGs), by using the power electronics, energy generation and storage systems can be coupled via a DC bus [2]. In such a configuration, the FESS ensures the DC-bus voltage control, thus contributing to the generation/consumption balance. The power converter connected to the network can then be concerned with the mains voltage and frequency control, and the wind generator can contribute to the ancillary services.

For accomplishing these objectives, a generating system, which must be able to feed isolated loads or to be integrated in the network, is here considered. The wind generator must then work without auxiliary source to contribute to the generation/ consumption balance, and to set the adequate frequency and voltage. A FESS is linked to the DC bus. The connection to the network is achieved through a LC filter and a transformer. The LC filter ensures a good voltage quality, and is well suited for feeding isolated loads. The reference value of the power generated to the network can be determined by means of a fuzzy-logic supervisor and the voltage and frequency control is achieved using resonant controllers [3] - [6].

In general, for a FESS associated to a VSWG, the restrictions in mass and volume are not crucial, and the flywheel is built from steel, for a maximum rotational speed of 10,000 rpm [1], [7]. Magnetic bearings and vacuum are not necessary. A low-speed FESS, whose electric machine is a classical squirrel-cage induction machine, is considered in this paper. FESS is connected to the DC bus of the system in order to control the power flow from the VSWG to the network. The study is concerned with the FESS efficiency and dynamic performance.

II. VSWG-FESS SYSTEM UNDER STUDY

Fig. 1 shows the VSWG-FESS system under study. It is scale-modeled by the laboratory test bench schematized in Fig. 2, which is currently developed at the Ecole des Hautes Etudes d'Ingenieur (HEI) Lille, France. The test bench has a modular structure, allowing the study of different VSWG-FESS system topologies. The wind turbine is emulated by a DC machine (3 kW / 1500 rpm), fed through a PWM converter entailing a DS1104 dSPACE™ card (PowerPC 603e / TI DSP TMS320F240) control. It drives a permanent-magnet synchronous generator (2.8 kW / 3000 rpm), whose stator is connected to the DC bus (3300 µF / 800V) through a PWM rectifier. This one, similarly to the grid-connected PWM inverter, is controlled by a DS1103 dSPACE™ Card (PowerPC 604e / TI DSP TMS320F240). Lastly, the squirrel-cage induction machine (3 kW / 1500 rpm), coupled to a flywheel (0.2085 $kg \cdot m^2$), is powered by a DS1104 dSPACE™ card-controlled PWM converter.

All the PWM converters have the same structure, and are provided with SEMIKRON™ IGBTs (1200V/50A). Control and measurement interfaces between converters dSPACE™ cards and sensors make possible configuration changes.

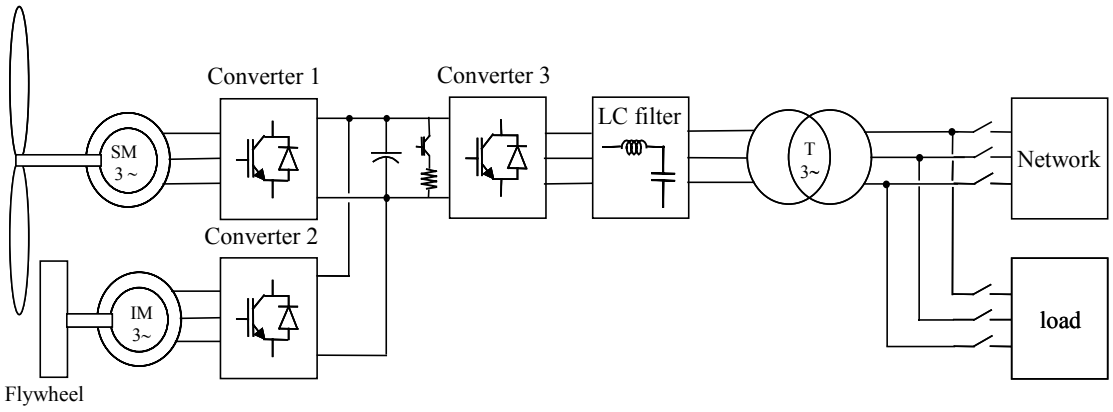

Fig. 1. VSWG-FESS system under study

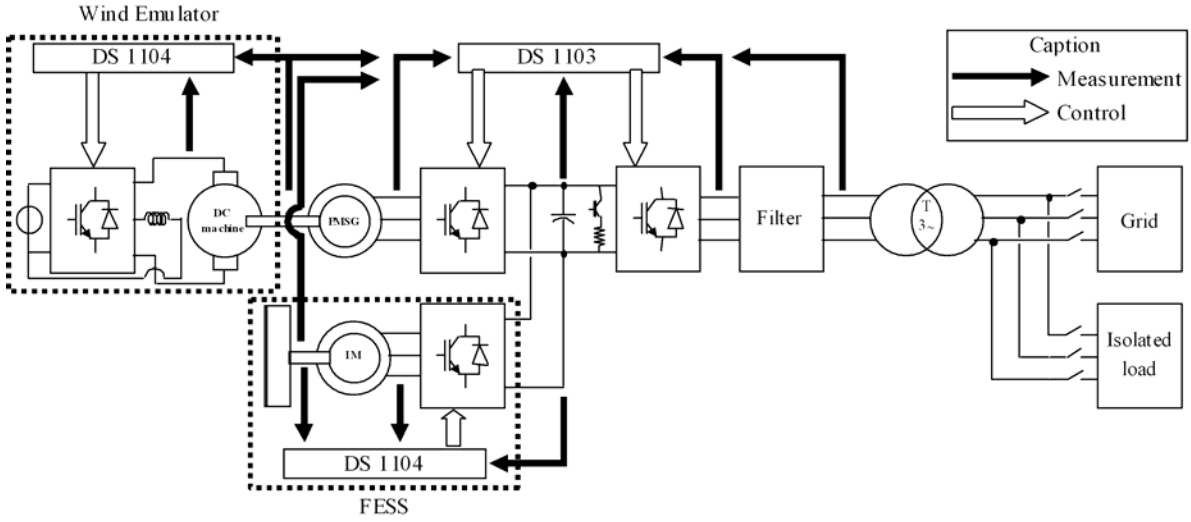

Fig. 2. Scheme of the experimental test bench

The developed test bench allows investigations of grid-connected or isolated load-connected energy generation and storage systems. Several grid connections can be thus considered with reference to the filter (L, LC etc.) used, so that different control strategies, accounting for likely unbalanced energy flows, can be implemented.

III. FESS Losses And Efficiency

A. FESS electronic power converter losses and efficiency

The dissipated power on the IGBT operating in the switching mode may be expressed by

$$P = \frac{1}{T} \cdot \int_0^T V_{CE}(t) \cdot i(t) \cdot dt \ , \qquad (1)$$

where T is the signal period, V_{CE}, the drop voltage on the IGBT, and i, the electric current crossing the IGBT.

1) *Switching losses.* For an IGBT power converter leg (Fig. 4), the commutation losses can be expressed by [9], [10]

$$p_{com} = \left(k_{Won} \cdot W_{on}(i) + k_{Woff} \cdot W_{off}(i)\right) \cdot f_{pwm} \ , \qquad (2)$$

where $W_{on}(i)$ and $W_{off}(i)$ are the turn-on and turn-off dissipated energy characteristics for the IGBT, respectively; in this case, $k_{Won} = k_{Woff} = V_{dc} / E_W$ with V_{dc}, the voltage of the DC-link circuit and E_W, the manufacturer's laboratory test voltage.

The total commutation losses of the FESS three-phase bridge-type power converter are obtained by trebling p_{com} of Eq. (2).

2) *Conduction losses.* Fig. 3 shows the electric current at one terminal of the power converter for a positive half-period; the IGBT conductperioT_{IGBT},and of the diode, T_D, are presented, for a PWM period T_{PWM}.

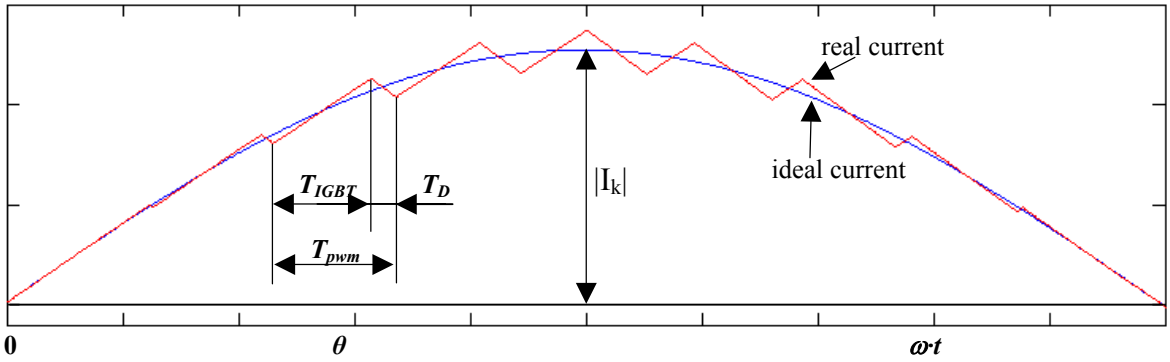

Fig. 3. Positive half-period of the current waveform at the power-converter leg terminal

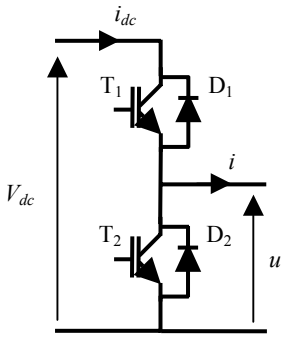

Fig. 4. Structure of a power converter leg

If the PWM frequency is sufficiently high, it can be considered that, for an electrical period, the cyclic ratio for a power converter leg is

$$\rho = \frac{1}{2} + \frac{r \cdot \sin(\theta + \varphi)}{2} = \frac{T_{IGBT}}{T_{pwm}} = T_{IGBT} \cdot f_{pwm}\,, \qquad (3)$$

where $f_{pwm} = 1/\ T_{pwm}$, r denotes the modulation depth and cosφ, the power factor. Some values for ρ are given in Fig. 5.

It should be noted that the dead time of the power converter is not considered in this study.

So, the conduction periods of the IGBTs and diodes, during a PWM period, are, respectively:

$$T_{IGBT} = \frac{\rho}{f_{pwm}} = \left(\frac{1}{2} + \frac{r \cdot \sin(\theta + \varphi)}{2}\right) \cdot T_{pwm}\,, \qquad (4.a)$$

$$T_D = \frac{1 - \rho}{f_{pwm}} = \left(\frac{1}{2} - \frac{r \cdot \sin(\theta + \varphi)}{2}\right) \cdot T_{pwm}\,. \qquad (4.b)$$

It has been assumed a sinusoidal shape of the current by neglecting its overlapped waves, i.e. $i = |I_k| \cdot \sin\theta$ [8]. Moreover, the current is supposed constant during the PWM period, and only the positive half-period of the current is considered for the losses computation (for the second half-period of the current, the losses being the same).

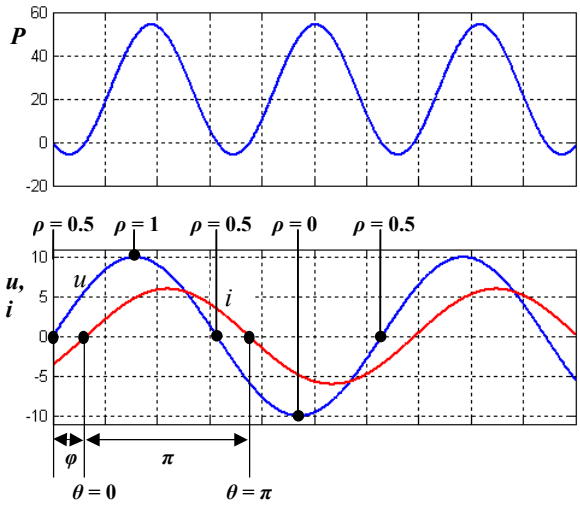

Fig. 5. Waveforms of the voltage, u, current, i, and power, P

The dissipated energy in the IGBT, during one PWM period and for an angle θ, is given by

$$E_{TR} = V_{ce} \cdot |I_k| \sin\theta \cdot \left(\frac{1}{2} + \frac{r \cdot \sin(\theta + \varphi)}{2}\right) \cdot T_{pwm}\,, \qquad (5)$$

where V_{ce} is the voltage drop on the IGBT in the switch-on mode. The dissipated power in the IGBT, for an angle θ, is

$$P_{TR} = V_{ce} \cdot |I_k| \sin\theta \cdot \left(\frac{1}{2} + \frac{r \cdot \sin(\theta + \varphi)}{2}\right). \qquad (6)$$

Fig. 5 shows that the power has a double pulsation as compared to the voltage or the current. Therefore, the average dissipated power in the IGBT can be written as

$$P_{IGBT} = \int_0^{\pi} V_{ce} \cdot |I_k| \sin\theta \cdot \left(\frac{1}{2} + \frac{r \cdot \sin(\theta + \varphi)}{2}\right) \cdot d\theta\,, \qquad (7)$$

leading to

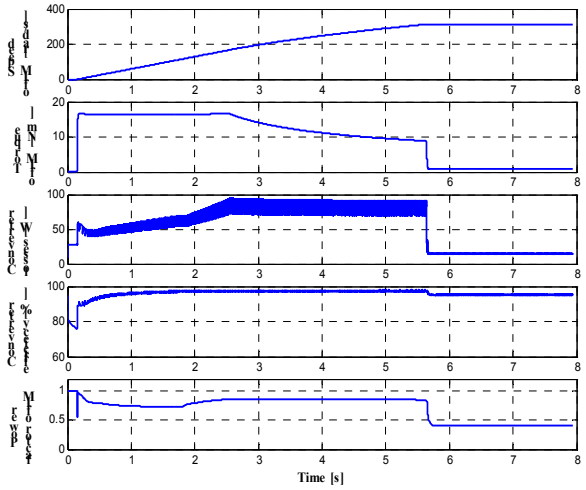

Fig. 6. Losses and the efficiency of the FESS power converter
during acceleration from standstill to maximum speed

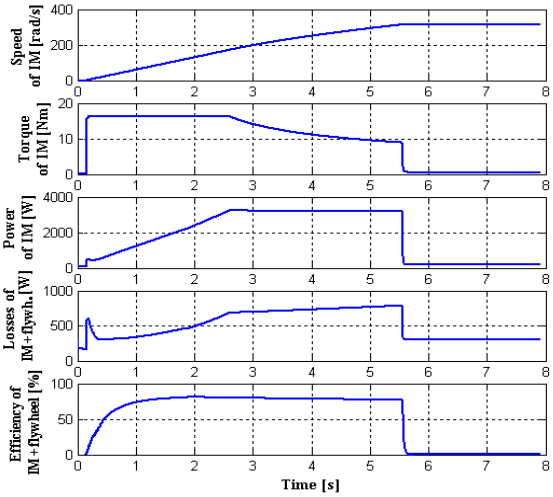

Fig. 7. Losses and the efficiency of the FESS IM-plus-flywheel during acceleration from standstill to maximum speed

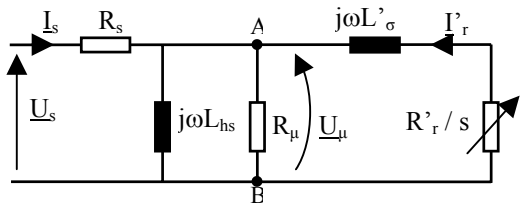

Fig. 8. Equivalent diagram of the IM

$$P_{IGBT} = V_{ce} \cdot |I_k| \cdot \left(\frac{1}{\pi} + \frac{r \cdot \cos\varphi}{4} \right). \tag{8}$$

In the same way, the diode conduction losses can be written as

$$P_D = V_D \cdot |I_k| \cdot \left(\frac{1}{\pi} - \frac{r \cdot \cos\varphi}{4} \right), \tag{9}$$

where V_D is the voltage drop on the diode. Eqs. (8) and (9) determine the conduction losses for one leg of the power electronic converter. Hence, the total conduction losses of the FESS power converter are given by the Eq. (10).

By summing the commutation and conduction losses given by Eq. (2) and Eq. (10), respectively, one obtains the total losses of the FESS power converter.

The characteristics of the SKM 50 GB 123 D IGBT module, provided by SEMIKRON, have been used in the simulation of a FESS power converter with a PWM frequency set at 8 kHz. Fig. 6 shows the simulation results.

$$p_{cond} = 3 \cdot (P_{IGBT} + P_D) = 3 \cdot |I_k| \cdot \left(\frac{V_{ce} + V_D}{\pi} + r \cdot \cos\varphi \cdot \frac{V_{ce} - V_D}{4} \right). \tag{10}$$

B. FESS IM-plus-flywheel losses and efficiency

1) *Stator copper losses* are computed by using the stator resistance R_s and the Park components of the stator current:

$$p_{JS} = R_s \cdot (i_{sd}^2 + i_{sq}^2). \tag{11}$$

2) *Rotor copper losses* can be written as the product of the electric power P and the slip s of the IM:

$$p_{JR} = s \cdot P = s \cdot (v_{sd} \cdot i_{sd} + v_{sq} \cdot i_{sq}). \tag{12}$$

3) *Iron losses* are determined from the IM equivalent diagram of Fig. 8:

$$p_{Fe} = 3 \cdot \frac{(U_s \cdot \cos\varphi - R_s \cdot I_s)^2 + (U_s \cdot \sin\varphi)^2}{R_\mu}. \tag{13}$$

It should be noted that Eq. (13) calculates the IM iron losses for a sinusoidal regime by neglecting the PWM losses.

4) *Friction losses* are determined as

$$p_f = \Omega_{\mathrm{IM}} \cdot (T_s + \Omega_{\mathrm{IM}} \cdot B), \tag{14}$$

where T_s is the static torque, B, the viscous friction coefficient and Ω_{IM}, the mechanical speed.

Fig. 7 gives the simulation results for the total losses and efficiency of the FESS IM-plus-flywheel.

It can be seen from Fig. 6 that the FESS power converter efficiency is influenced by the IM power factor. If the IM operates at rated power in the flux-weakening region, its power factor reaches the maximum value 0.86 and the converter efficiency is 97.5 %, whereas the efficiency of the IM-plus-flywheel is around 82 %.

IV. Experimental Results

In this section, the experiments carried out using the test bench of Fig. 2 are presented in order to validate the previous simulation results. In the considered case, the FESS is not coupled with the VSWG. The flywheel is accelerated to the maximum speed and stores the energy from the network. Then, the flywheel brakes and delivers through the IM its energy into the network.

The IM coupled to the flywheel operates in the field-weakening region, as having the rotor speed between 1500 and 3000 rpm. The corresponding IM power equation is determined as

$$P_{\mathrm{IM}} \approx T_{em\,\mathrm{IM}} \cdot \Omega_{\mathrm{IM}} = p \cdot \frac{M}{L_r} \Phi_{rd} \cdot i_{sq} \cdot \Omega_{\mathrm{IM}} \qquad (15)$$

with P_{IM}, the electric power, $T_{em\mathrm{IM}}$, the electromagnetic torque, Ω_{IM}, the mechanical speed, p, the pole-pair number, M, the mutual inductance, L_r, the rotor inductance, Φ_{rd}, the d-axis rotor-flux component, i_{sq}, the q-axis stator-current component.

From Eq.(15), the rotor-flux reference value can be computed as

$$\Phi_r(\Omega_{\mathrm{IM}}) = \frac{P_{\mathrm{IMr}} \cdot L_r^*}{p \cdot M^* \cdot i_{sq\max}} \cdot \frac{1}{\Omega_{\mathrm{IM}\,mes}}, \qquad (16)$$

where P_{IMr} is the IM rated power and $\Omega_{\mathrm{IM}mes}$, the IM measured speed. In Eq. (16), the IM parameters assigned with asterisk define the estimated parameters.

Since IM losses have been neglected in deriving Eq. (16), several values for P_{IMr} have been considered in order to assess the influence of this parameter on the IM-based FESS efficiency. Moreover, different values for P_{IMr} have been considered in function of the two operating modes of the IM, i.e. motor and generator. The experimental results have proven that the P_{IMr} value has a notable influence on the FESS efficiency.

Figs. 9 and 10 show the experimental efficiencies of the IM and of the power converter, for two values of P_{IMr}. Fig. 9 presents the case where P_{IMr} was set to the rated power of the IM. The experimentally-resulted IM-plus-flywheel efficiency was about 81 % in the charge operation and 72 % in the discharge operation. The efficiency of the DC-link power converter was about 95 % in the charge operation, and 86 % in the discharge operation.

In the second case (Fig. 10), the estimated losses of the FESS were added to the rated power of the IM and used to compute the rotor-flux reference value. So, the experimental efficiency of the IM-plus-flywheel was notably increased to 88 % in the charge operation and to 81 % in the discharge operation. The resulted DC-link power converter efficiency was also significantly improved to 91 % in the charge operation and to 92 % in the discharge operation.

Figs. 11 to 21 show the experimental results in the case when the FESS losses were considered for computing the rotor-flux reference value.

From Eq. (16), it can be written

$$i_{sq\,ref} = \frac{P_{\mathrm{IMr}} \cdot L_r^*}{p \cdot M^* \cdot \Phi_r(\Omega_{\mathrm{IM}})} \cdot \frac{1}{\Omega_{\mathrm{IM}\,ref}}, \qquad (17)$$

where $i_{sq\ ref}$ is the reference current for the IM's current regulator. This relation was used to compute the reference current in function of the desired operating power for the IM, in order to carry out the experiments at the different IM power values, P_{IMr}.

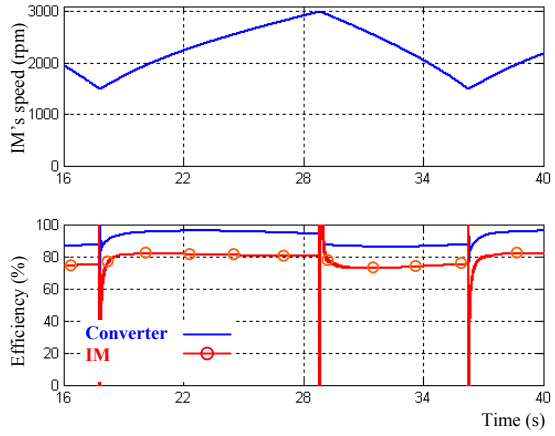

Fig. 9. Experimental efficiency of the FESS for P_{IMr} = 3000 W

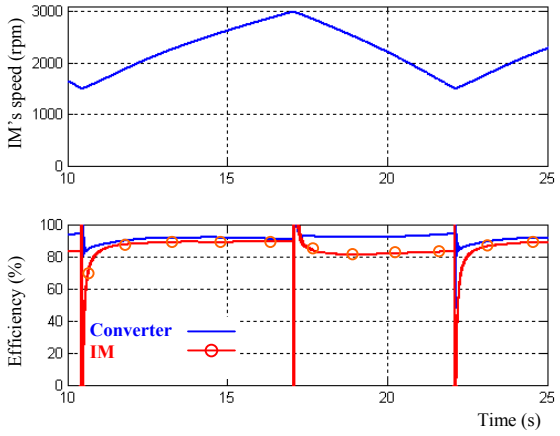

Fig. 10. Experimental efficiency of the FESS for P_{IMr} = 3700 W

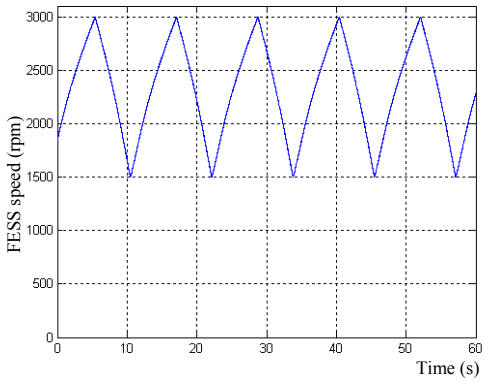

Fig 11. FESS speed

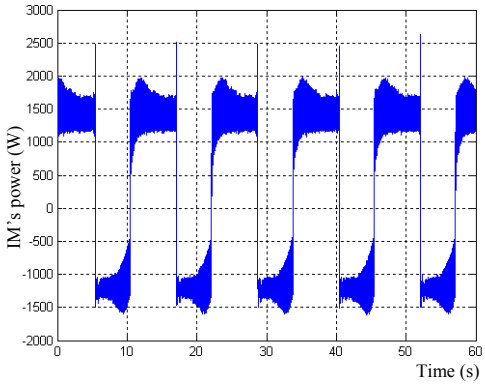

Fig. 12. IM's active power

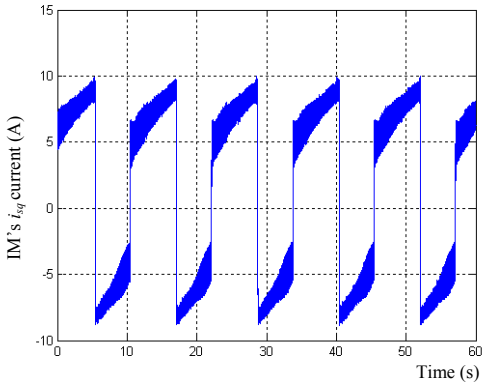

Fig. 13. IM's i_{sq} current

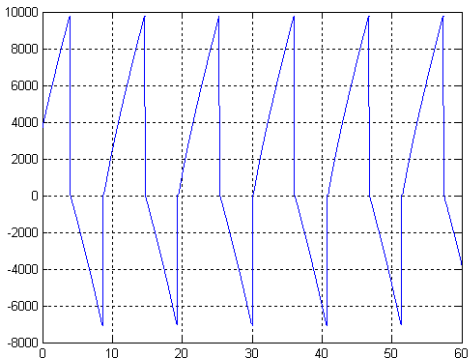

Fig. 14. FESS energy measured at the network side

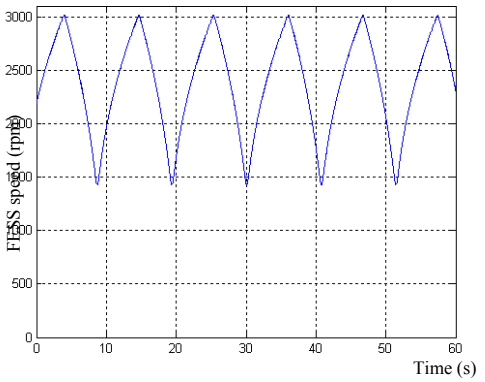

Fig 15. FESS speed

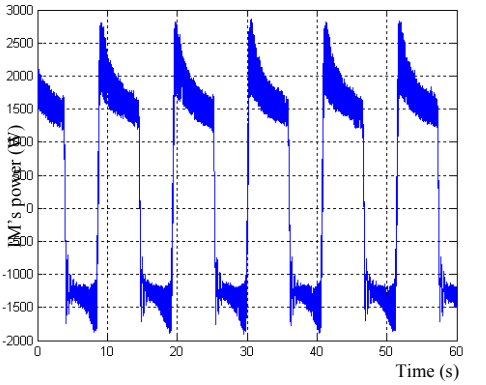

Fig. 16. IM's active power

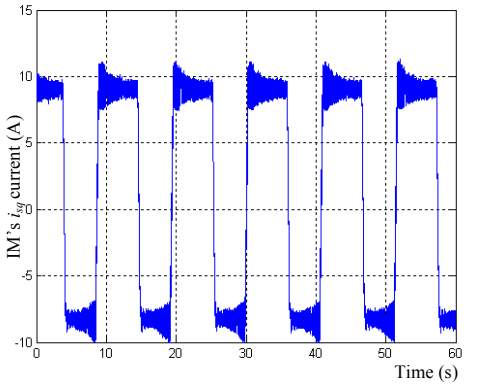

Fig. 17. IM's i_{sq} current

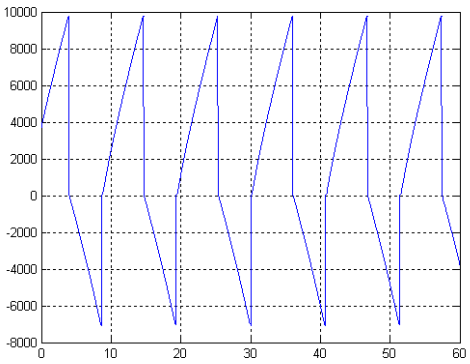

Fig. 18. FESS energy measured at the network side

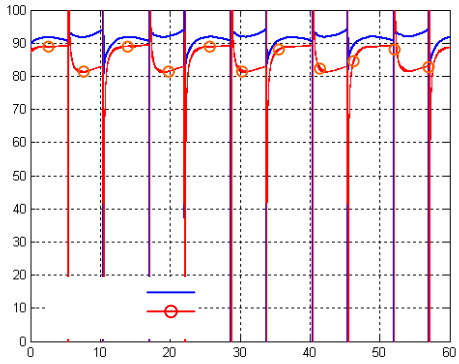

Fig. 19. IM and DC-link converter efficiencies

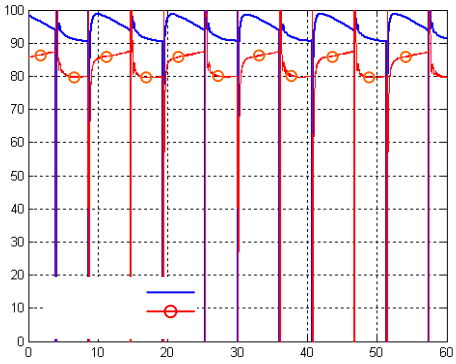

Fig. 20. IM and DC-link converter efficiencies

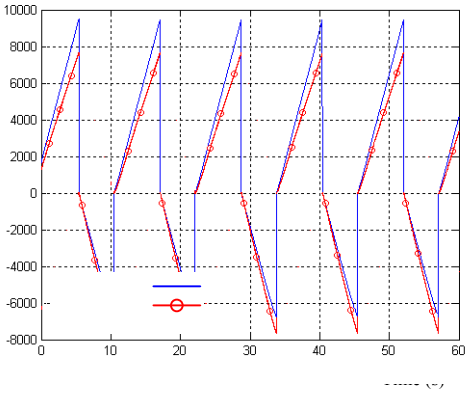

Fig. 21. FESS energy measured at the network side and the flywheel's kinetic energy

Moreover, two cases for the speed value $\Omega_{\mathrm{IM}\,ref}$, were considered in Eq.(17). In the first case (figures 11 to 14), the speed reference was set to a constant value of 314 rad/s. In the second case (figures 15 to 18), the measured values of speed were used in the real-time computation of the $i_{sq\,ref}$ current.

By integrating the electric power of the FESS, the energy stored/delivered in/from the flywheel can be computed. Thus, the FESS efficiency can be written as

$$\eta_{FESS} = \left|\frac{E_d}{E_s}\right| \cdot 100 \ [\%], \tag{18}$$

where E_s and E_d are the energy stored/delivered in/from the flywheel, respectively, both estimated for one charge/discharge cycle [11]. For the both cases discussed above, the FESS efficiency was about 71 %, but the separate IM and power converter efficiencies are very different (as can be seen in Figs. 19 and 20).

The kinetic energy stored in the flywheel is given by

$$E_{fly} = J\frac{\Omega_{\mathrm{IM}}^2}{2}, \tag{19}$$

(J is the FESS inertia) and can be shown in the Fig. 21 in comparison with the network-side measured energy.

There are significant differences between the DC-link converter efficiencies in the two considered cases of Figs. 20 and 21. From both figures, it also results that the efficiency of the DC-link converter is strongly dependent on the IM control strategy. Particularly, the experiments had proved that the flux-weakening strategy has an important influence on the IM and the DC-link converter efficiencies [12].

V. Conclusion

In this paper, the performance analysis of an IM-based FESS associated to a VSWG has been presented. The electronic power converter and the IM-plus-flywheel have been separately considered for the FESS losses and efficiency determination. Good agreement between simulation and experimental results has been found.

VI. Appendix

A. IM-plus-flywheel parameters

Number of poles: $2{\cdot}p = 4$;
Stator resistance: $R_s = 0.76\ \Omega$;
Rotor resistance: $R_r = 0.76\ \Omega$;
Core loss resistance: $R_\mu = 293.3\ \Omega$;
Magnetizing inductance: $M = 77.67$ mH;
Leakage inductance: $L_\sigma = 7.30$ mH;
Stator inductance: $L_s = 81.32$ mH;
Rotor inductance: $L_r = 81.32$ mH;
Total leakage factor: $\sigma = 0.071$;
Rated current: $I = 10.9$ A;
FESS inertia: $J = 0.2085$ kg·m^2;
Viscous friction coefficient: $B = 0.0011$ Nm·s·rad^{-1}.

B. Network connection

Filter: Inductance: $L_f = 3$ mH;

Resistance: $R_f = 0.1\ \Omega$;

Transformer:

Equivalent leakage inductance: $L_{tr} = 0.923$ mH;

Equivalent winding resistance: $R_{tr} = 1.18\ \Omega$.

C. DC-link parameters

Capacity: $C = 3300\ \mu F$;
Maximal voltage: $V_{dc\max} = 800$ V.

D. Power converter parameters

All the power converters are provided by SEMIKRON^{TM} and are composed from a SKD 51/14 rectifier module, three SKM 50 GB 123 D and one SKM 50 GAL 123 D IGBT modules whose parameters are fully given at http://www.semikron.com .

ACKNOWLEDGEMENT

This work was supported in part by the Romanian Ministry of Education, Research and Youth.

REFERENCES

[1] R. Hebner, J. Beno, A. Walls, "Flywheel batteries come around again", IEEE Spectrum, April 2002, pp. 46-51.

[2] R. Cardenas, R. Pena, G. Asher, J. Clare, "Control strategies for enhanced power smoothing in wind energy systems using a flywheel driven by a vector-controlled induction machine", IEEE Transactions on Industrial Electronics, vol. 48, n° 3, June 2001, pp. 625-635.

[3] L. Leclercq, B. Robyns, J.M. Grave, "Fuzzy logic based supervisor of a flywheel energy storage system associated with wind and diesel generators", Proceedings of the 8th International Conference on Optimization of Electrical and Electronic Equipments - OPTIM 2002, Brasov, Romania, May 2002, vol. II, pp. 441-446.

[4] L. Leclercq, B. Robyns, J.M. Grave, "Control based on fuzzy logic of a flywheel energy storage system associated with wind and diesel generators", Mathematics and Computers in Simulation, 63, 2003, pp.271-280.

[5] L. Leclercq, A. Ansel, B. Robyns, "Autonomous high-power variable-speed wind generator system", 10th European Conference on Power Electronics and Applications, EPE 2003, 2-4 September 2003, Toulouse, France.

[6] L. Leclercq, C. Saudemont, B. Robyns, G. Cimuca, M.M. Radulescu, "Flywheel energy storage system to improve the integration of wind generators into a network", ELECTROMOTION, vol. 10, n° 4, 2003, pp. 641-646.

[7] F. Hardan, J. A. M. Bleijs, R. Jones, P. Bromley, "Bi-directional power control for flywheel energy storage system with vector-controlled induction machine drive", IEE conference publication, pp. 456-477, 1998.

[8] C. Rivas, A. Rufer, Comparaison des pertes des convertisseurs pour systèmes de production d'énergie électrique à partir d'une pile à combustible, Actes de 8ème Colloque « Electronique de Puissance de Futur » – EPF 2000, 29 nov. – 1 déc. 2000, Lille, France, pp. 239 – 243.

[9] T. Brückner, S. Bernet, "Investigation of a Hight-power Three-Level Quasi-Resonant DC-Link Voltage-Source Inverter", IEEE Transaction on Industry Application, Vol. 37, No. 2, March / April 2001.

[10] P. Bastiani, "Stratégies de commande minimisant les pertes d'un ensemble convertisseur – machine alternative: Application à la traction électrique", Ph.D. dissertation, Institut National des Sciences Appliquées de Lyon, Lyon, France, 2001.

[11] P. Tsao, S.R. Sanders, "An Integrated Flywheel Energy Storage System With Homopolar Inductor Motor/Generator and High-Frequency Drive", IEEE Transaction on Industry Application, Vol. 39, No. 6, November / December 2003.

[12] F. Abrahamsen, F. Blaabjerg, J.K. Pedersen, P.B. Thoegersen, "Efficiency-Optimized Control of Medium-Size Induction Motor Drives", IEEE Transaction on Industry Application, Vol. 37, No. 6, November / December 2001.